RADIO SCIENCE, VOL. 48, 1–12, doi:10.1029/2012RS005074, 2013

A comprehensive sounding of the ionospheric HF radio link from Antarctica to Spain

A. G. Ads,[1] P. Bergadà,[1] C. Vilella,[1] J. R. Regué,[1] J. L. Pijoan,[1] R. Bardají,[1] and J. Mauricio[1]

Received 16 July 2012; revised 16 October 2012; accepted 15 November 2012; published 24 January 2013.

[1] Since 2003, our group has been investigating the performance of different transmission techniques for low-power low-interference High Frequency (HF) ionospheric communication systems. Specifically, we have focused on the link between the Spanish Antarctic Station (SAS) Juan Carlos I in Livingston Island and Ebro Observatory (OE) in Spain, in order to transmit the data gathered from some geomagnetic sensors. These transmission techniques require a valuable knowledge of the channel behavior, thus a comprehensive narrowband and wideband sounding of the ionospheric channel is needed. Some significant improvements both in the system and in the signal processing have been done to achieve this goal. The analysis time and the frequency band have been extended to 24 hours per day and to the whole HF band (2-30 MHz). Moreover, new measurements of the absolute propagation time and the Doppler frequency shift are introduced. In this paper, the sounding results obtained using the new system are presented.

Citation: Ads, A. G., P. Bergadà, C. Vilella, J. R. Regué, J. L. Pijoan, R. Bardají, and J. Mauricio (2012), A comprehensive sounding of the ionospheric HF radio link from Antarctica to Spain, *Radio Sci.*, *48*, 1–12, doi:10.1029/2012RS005074.

1. Introduction

[2] The ionospheric HF communications channel is a special case of slow fading multipath channel where both digital communications concepts and geophysical knowledge are required. The refraction of HF waves (2-30 MHz) in the ionized medium makes propagation over long distances possible up to 3000 km per reflection hop. HF communications are very useful for military purposes, fleet control and communications with remote areas, where no satellite coverage is available.

[3] Communications from North and South poles underlines the importance of skywave propagation in the HF band since line of sight from geostationary satellite is not feasible. In that sense, our Research Group is developing a new communication system from the SAS to Spain in order to transmit the data from remote sensors installed in Livingston Island (South Shetland Islands), Antarctica to the OE in Roquetes, Spain.

[4] The research project started in 2003 with three main objectives:

1. Channel sounding and modeling, taking into account the daily, annual, and solar cycle variations.
2. Design of the best digital modulation scheme for a low-power, low-interference communication system.
3. Implementation of robust hardware and software able to operate under hard environmental conditions.

[5] A more detailed description of this project can be found in *Bergadà et al*. [2009].

[6] Previous work, mainly in mid-latitudes and polar regions, is revised in *Vilella et al*. [2008]. [*Angling et al*., 1998; *Warrington*, 1998] added important contributions for high-latitudes, [*Angling and Davies*, 1997; *Warrington and Stocker*, 2003] in mid-latitudes, and [*Houpis and Nickisch*, 1991; *Fitzgerald et al*., 1999] introduced results for low-latitudes.

[7] The first channel model, widely accepted for narrowband transmissions, was developed by *Watterson et al*. [1970]. *Vogler and Hoffmeyer* [1993] from Institute of Telecommunication Science (ITS) developed a wideband ionospheric HF channel model with non Gaussian statistics and delay spread parameters. *Mastrangelo et al*. [1997] provided an HF channel simulation system that is well operative with both narrowband and wideband HF channels model.

[8] The hardware of the channel sounder and the radio modem has been updated several times since the 2003/2004 survey. Three main Software Defined Radio (SDR) platforms have been installed in both the transmitter and the receiver. The first one, Sounding System for Antarctic Digital Communications (SANDICOM) is described by *Vilella et al*. [2005].

[9] During the 2005/2006 survey, the second generation SODIO started with a new digital platform using Field

[1]Grup de Recerca en Electromagnetisme i Communicacions (GRECO), La Salle, University of Ramon Llull, Barcelona, Spain.

Corresponding author: A. G. Ads, Grup de Recerca en Electromagnetisme i Communicacions (GRECO), La Salle, University of Ramon Llull, 30 Barcelona, 08022 Spain. (aads@salle.url.edu)

©2012. American Geophysical Union. All Rights Reserved.
0048-6604/13/2012RS005074

Programmable Gate Arrays (FPGA), and an Application Specific Integrated Circuits (ASIC) with high speed Digital to Analog Converter (DAC) as explained by *Vilella et al*. [2006]. The results obtained by the SODIO system have been introduced by *Vilella et al*. [2008]. The system had some limitations in both sounding time (00:00 UTC to 11:00 UTC and 18:00 UTC to 23:00 UTC), frequency (4.5 MHz to 16.5 MHz), and also in the measurement capabilities. For these reasons, the daytime data, propagation time, and Doppler frequency shift could not be obtained. The limitation of the operating time of the system to 18 hours was due to changing the configuration of the system which carried out manually by the staff in the SAS.

[10] Finally, in the 2009/2010 survey (November 2009 to February 2010), a third generation platform called POTASIO was installed in both the SAS and OE. The new system is easier to handle and maintain than the previous one, and is able to operate during 24 hours per day with an extended frequency range from 2 MHz to 30 MHz. Therefore, the results presented in this paper represent a substantial improvement to the previous work.

[11] First, a brief description of the link and the hardware is given. Next, the description of the narrowband and wideband analysis methodologies is provided. Finally, the results from both the narrowband, wideband sounding, propagation time, and Doppler frequency shift are presented.

2. Link Description

[12] One of the main objectives of our work is to establish a permanent HF link between the SAS in Livingston Island (62.6S, 60.4 W) and OE (40.8 N, 0.5E). The distance between the SAS and OE is approximately 12700 km. Hence, according to *Davies* [1990], a minimum of four hops are needed. The coordinates of these hops are listed in *Vilella et al*. [2008]. The propagation conditions are strongly depend on sun radiation, so daily, seasonal, and solar cycle variations have to be studied. Furthermore, the equatorial anomaly, the auroral electrojet, and the variation of sunset time along the path influence on the channel behavior. Regarding interferences and multipath, a study of quiet frequencies has been made in order to avoid strong signals from broadcast stations, ionosondes, and other HF services.

[13] In some subbands, echoes from different layers reflection, and even propagation throughout the long path, i.e., along the other side of the Earth, increase the time-delay spread of the channel, and so reducing the coherence bandwidth.

[14] As there are few studies of such long-haul links, our group has been measuring all the significant channel parameters both in narrowband and wideband conditions since 2003 in order to have a complete historical series.

3. System Description

[15] As previously mentioned, the hardware of the channel sounder and data transmission system has been updated in order to extend the frequency range and measuring capabilities and improve the frequency and time accuracy. Therefore, the whole transmission system is totally redesigned and reequipped with faster and more reliable equipments during the 2009/2010 survey. Now, the system is able to operate at a higher bandwidth up to 40 kHz and sampling rate up to 100 ksps. This allows the system to be completely flexible in selecting the most suitable bandwidth for every type of transmission. The main features of the transmitter and receiver hardware, as well as the data frame structure are summarized below.

3.1. Hardware of the Transmitter

[16] The core of the system is a digital platform with an embedded PC with a Digital Signal Processing (DSP) unit inside, that performs the tasks of system control and parameter configuration. The main DSP unit (*XTremeDSP-IV*) from XILINX includes three FPGA. The first FPGA (*Virtex-II*) is responsible for configuring the clock. The main FPGA (*Virtex-4*) equipped with two 14-bit Analog to Digital Converter (ADC), two 14-bit DAC, and all the arithmetic and peripherals drivers, performs the software radio procedures. Finally, a preconfigured FPGA (*Spartan-II*) handles the interface between the PCI bus and the *Virtex-4*. A block diagram of the transmitter is shown in Figure 1.

[17] A new GPS unit with the Pulse per Second (PPS) signal increases the time synchronization accuracy (1 μs), making the measurement of the propagation time of the wave possible. In order to improve the frequency synchronization accuracy, a 100 MHz Oven Controlled Crystal Oscillator (OCXO) is installed in both the transmitter and the receiver side. Moreover, the transmitter power amplifier can be switched off in case of severe impedance mismatch by means of a wattmeter that controls the forward and reverse transmitted power.

[18] All the transmitter hardware is deployed close to the antenna at the top of a hill near to the SAS. All the electronics are inside a watertight sealed box, which provides electromagnetic shielding and protection against hard weather conditions. The system is remotely accessed by using a Wireless Local Area Network (WLAN) from the laboratory in the SAS.

3.2. Hardware of the Receiver

[19] The receiver, whose block diagram is shown in Figure 2, uses the same digital platform as the transmitter. Monopole and Yagi are the antennas used to receive the signal. The Yagi is only used around 15 MHz, whereas the monopole is used along the whole HF band.

[20] As shown in Figure 3, the RF signal is passed through a Low Noise Amplifier (LNA) and two additional amplification stages. One of them is a digitally controlled Variable Gain

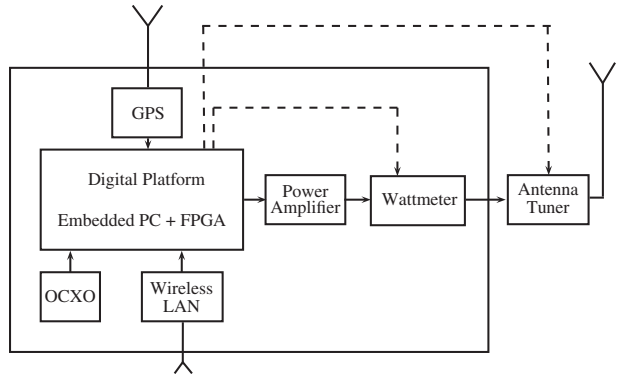

Figure 1. Block digram of the POTASIO transmitter side.

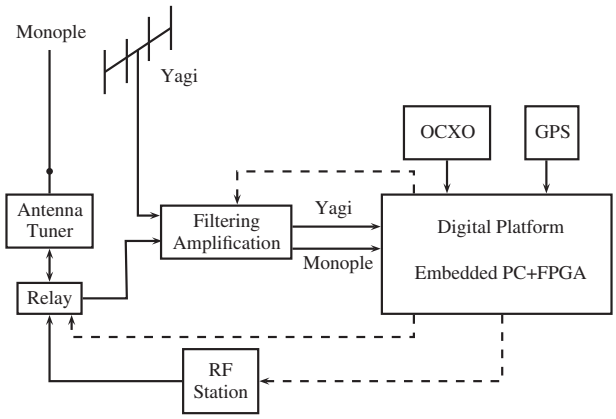

Figure 2. Block digram of the POTASIO receiver side.

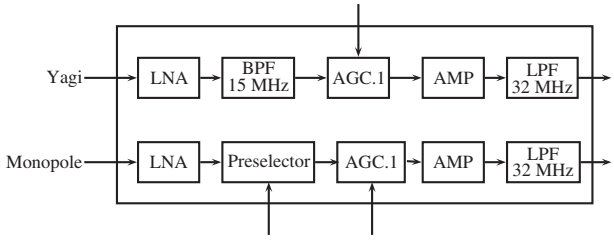

Figure 3. Filtering and amplification unit at the receiver side.

Amplifier (VGA) with a variable gain range of -5 dBto + 40 dB. The first filter for the RF signal received from the monopole is a preselector of three tunable filters that cover the whole HF band, while it is a fixed 15 MHz Band Pass Filter for the signal received from the Yagi. A 32 MHz antialiasing filter is at the end of the filtering and amplification unit.

[21] A commercial RF station is used to transmit a low power signal during a short period of time in order to tune the antenna tuner of the monopole antenna.

3.3. Frame Structure

[22] The signals to be transmitted are organized in a frame as shown in Figure 4. The waiting intervals are defined as W. After the antenna tunning period, a full power tone is transmitted during 10 seconds for narrowband sounding. This period is used for channel availability estimation and for computing the SNR statistics. After a 4 seconds waiting period, a pseudo random noise (PN) sequence (m-sequence) of variable length and with good autocorrelation properties, as discussed by *Parsons* [2000], is transmitted during 10 seconds for wideband sounding. The wideband channel parameters to be measured are wideband SNR, multipath spread, Doppler spread, propagation time, and Doppler shift.

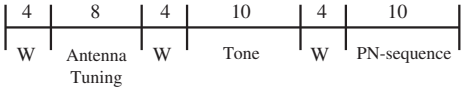

Figure 4. A simple transmitted frame.

4. Narrowband Analysis

[23] Narrowband analysis focuses on channel availability and SNR computation. The channel availability means the probability of a link to reach a minimum SNR value and hence achieve a certain quality of service as defined by *Goodman et al*. [1997]. According to *Vilella et al*. [2008] a minimum SNR value of 6 dB has been specified to estimate the channel availability in a bandwidth of 10 Hz. In this paper, we have improved the narrowband detection method by measuring the variation of the SNR along the received signal power profile. This is done by windowing and time framing the received signal in the time domain, as explained below. Such techniques improves the reliability of the detection system against noise and interference significantly.

[24] SNR is computed by comparing the received power P_s measured during the tone interval to the noise power P_n measured during the waiting periods. The problem that we are facing is the false detections produced by interference signals present during the signal interval. A summary of the survey configuration parameters is shown in Table 1.

4.1. Windowing

[25] In order to have a useful received signal power profile, the first step is to properly filter the received signal. In our case this is carried out in the frequency domain by multiplying the Fast Fourier Transform (FFT) of the received signal by the window frequency response. Such a filter has two main features:

1. It should eliminate signals at frequencies apart from the reception frequency.
2. It should have a good time response to avoid creating transients from the impulsive interferences that fall far away from the reception frequency.

[26] An example of a narrowband received signal filtered by an ideal rectangular window is shown in Figure 5, while a highly interfered one is shown in Figure 6. The window filter should deal with both cases. In the literature, several window function can be found. However for reasons of simplicity, we have just applied four windows which are Blackman (*Blackman et al*. [1959]), Hanning (*Blackman et al*. [1959]), Flattop (*Oppenheim and Shafer* [1989]), and Kaiser (*Kaiser* [1974]). A comparison between the four window functions is illustrated in Figure 7.

[27] The four window functions are applied to an interfered narrowband signal and outcomes are compared in Figure 6. The results of applying those windows are much better

Table 1. Configuration Setup for the Narrowband Sounding During the 2009/2010 Survey

	Configuration setup		
	1	2	
Sampling Frequency	100000		Hz
Time Interval	1–11	2–12	s
Guard Period	1		s
Window Filter	Kaiser		
Portion length	0.5		s
Threshold values	3, 6, 9, 15		dB

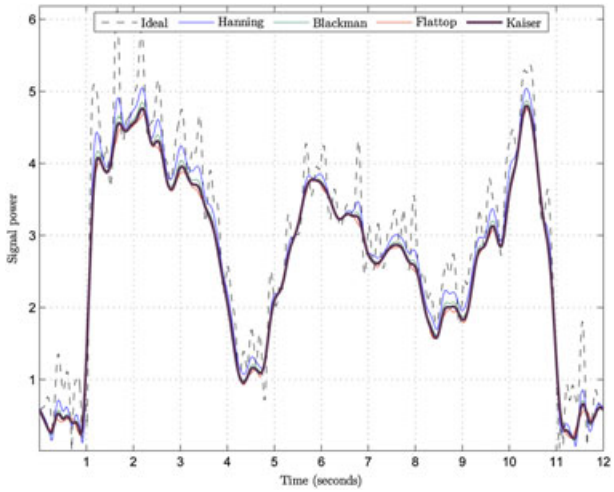

Figure 5. Narrowband signal filtered with the four different window functions with a carrier frequency of 15.5 MHz at 10:00 UTC.

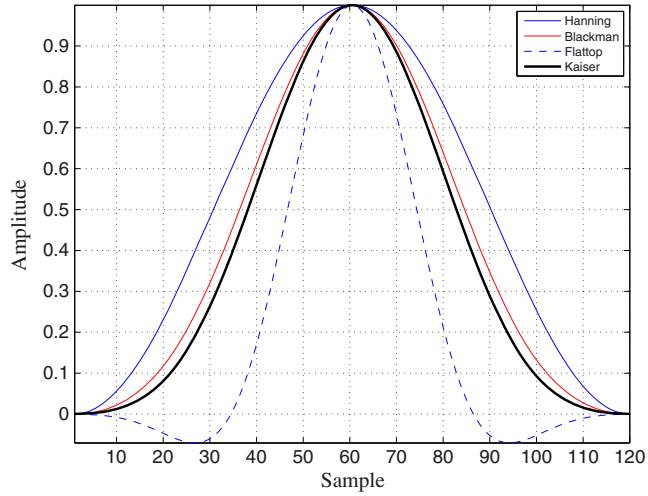

Figure 7. Time response of the four different window functions.

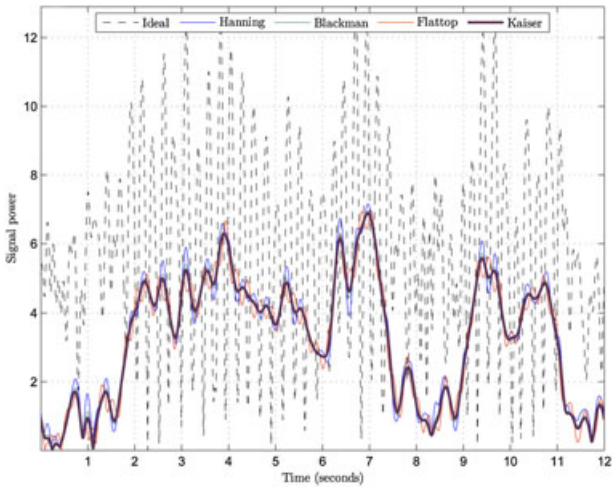

Figure 6. Ideal window compared with the other four window filters on a highly interfered narrowband signal with a carrier frequency of 20 MHz at 17:00 UTC.

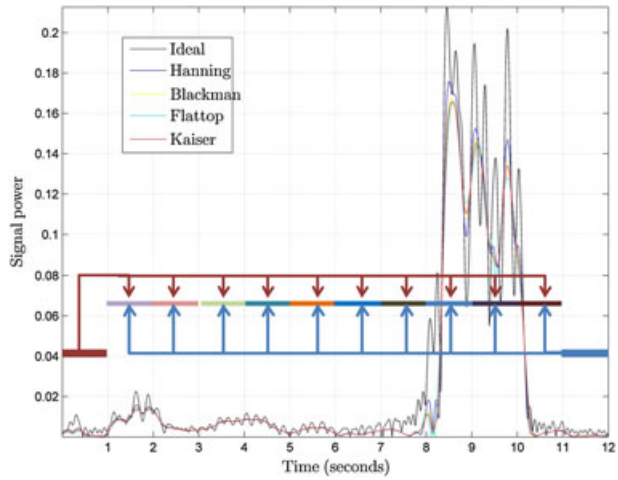

Figure 8. An example of high level interfered signal received during the tone period with a carrier frequency of 3 MHz at 00:00 UTC and the solution proposed to cancel its affect.

than the ideal one that was used in previous works by *Vilella et al.* [2008]. Kaiser window has a slightly better and smooth response than the rest of the windows, and is the window used in the rest of the work.

4.2. Time Framing

[28] SNR computation can be easily distorted by the presence of high-level interfering signals. In order to exclude the interfering signal from being considered as a good received signal, the presented time framing technique can be used. As shown in Figure 8, an interfering signal present during some seconds of the analyzed interval can lead to false SNR calculations.

[29] To overcome this problem, the whole received signal period was segmented into a certain number of periods, e.g., 10 periods in Figure 8. The SNR is computed as the ratio of the signal power on every segment over the noise power measured at the segments of the waiting period. So we have an evolution of the SNR along the observation interval. According to several previous experiments, two threshold values have been established, i.e., $Th_{low} = 3$dB and $Th_{high} = 6$dB. In order to have a high detection reliability, only measurements where SNR $\geq Th_{low}$ over 70% of the segments and SNR $\geq Th_{high}$ over 50% of the segments are considered to compute the availability and SNR estimations.

5. Wideband Analysis

[30] The wideband analysis is useful to characterize time and frequency dispersion channels and not only those that are slow and frequency dispersive. Seeking this goal, some PN sequences of different time length and bandwidth are transmitted. The configuration parameters used in the 2009/2010 survey are listed in Table 2.

Table 2. Configuration Setup for the Wideband Sounding During 2009/2010 Survey

Sampling Frequency	100000	Hz
Time Interval	1–11	s
Chip Frequency	5000	Hz
Sequence length	127	
Frequency spread window	(-4 4)	Hz
Time spread window	(-3 3)	ms
Minimum SNR threshold value	8	dB
Roll-off factor of the RCC filter	0.65	

[31] The received signal $r[n]$ is correlated with a copy of the original PN sequence S_e shaped by a raised cosine filter with a roll-off factor of 0.65 as illustrated in Figure 9. The correlation function $\phi_{r,S_e}[n]$ is calculated as:

$$\phi_{r,S_e}[n] = \sum_{k=0}^{N_e-1} r[n+k]S_e[k] \tag{1}$$

where N_e denotes the length of the PN sequence S_e. Therefore, the channel impulse response $h[n,\tau]$ can be expressed as:

$$\begin{gathered} h[n,\tau] = \phi_{r,S_e}[nlN_c + \tau], \\ n \in [0, \left[\frac{\Delta t F_m}{lN_c}\right] - 1], \\ \tau \in [0, lN_c - 1] \end{gathered} \tag{2}$$

where τ is the delay variable, l is the number of chips, N_c denotes the number of the samples per chip, Δt is the interval of the wideband sounding and F_m is the sampling frequency.

[32] From Equation 2, the following parameters are derived: scattering function, SNR, composite multipath spread, composite Doppler spread, propagation time, and Doppler frequency shift.

[33] The scattering function $R_s[\tau,v]$ is calculated as the FFT of the channel impulse response as explained by *Proakis* [2001]:

$$R_s[\tau, v] = \sum_{\xi} R_h[\xi, \tau] e^{-j2\pi\xi v} \tag{3}$$

where ξ denotes the time variable, v the Doppler frequency shift and

$$R_h[\xi, \tau] = \sum_{n} h^*[n, \tau] h[n + \xi, \tau] \tag{4}$$

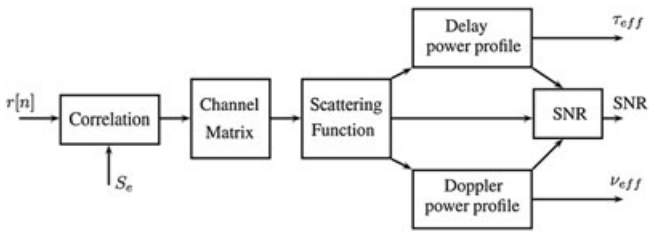

Figure 9. Block diagram of the algorithms applied in the wideband analysis.

[34] The time spread and frequency spread observation windows have been defined in Table 2 according to the results obtained by *Vilella et al*. [2008]. The power delay profile $\phi[\tau]$ is expressed by refining $R_s[\tau,v]$ along the Doppler window $[v_1,v_2]$ as:

$$\phi[\tau] = \sum_{v=v1}^{v2} R_s[\tau, v] \tag{5}$$

[35] In order to improve the robustness of the τ_c calculation, the power delay profile is modified by subtracting the average value of the squared noise. It should be noted that, if the observation window of multipath is well adjusted, $\phi[\tau]$ will contain the noise power outside the window. Therefore,

$$\tilde{\phi}[\tau] = \phi[\tau] - \frac{1}{T - (\tau_2 - \tau_1)} \sum_{m \notin [\tau_1, \tau_2]} \phi[m] \tag{6}$$

[36] Then, calculate the integral function of $\tilde{\phi}[\tau]$ can be expressed as:

$$\Phi(\tau) = \sum_{m=\tau_1}^{\tau_2} \tilde{\phi}[m], \quad \tau \in [\tau_1, \tau_2] \tag{7}$$

[37] So, the normalization of $\Phi(\tau)$ with respect to the maximum value defined as:

$$\bar{\Phi}(\tau) = \frac{\Phi(\tau)}{max(\Phi(\tau))} \tag{8}$$

[38] Finally, we obtain the value of delay by which $\bar{\Phi}(\tau)$ ranges between 10% and 90% of the maximum value:

$$\tau_{min} = \overset{min}{\tau}\, \bar{\Phi}(\tau) \geq 0.1 \tag{9}$$

$$\tau_{max} = \overset{max}{\tau}\, \bar{\Phi}(\tau) \leq 0.9 \tag{10}$$

[39] Hence, the composite multipath spread is expressed as:

$$\tau_c = \tau_{max} - \tau_{min} \tag{11}$$

[40] In a similar way, the Doppler power profile $\phi[v]$ is calculated from $R_s[\tau,v]$, averaged along the multipath window $[\tau_1 - \tau_2]$ as:

$$\phi[v] = \sum_{\tau=\tau_1}^{\tau_2} R_s[\tau, v] \tag{12}$$

[41] By using the same algorithm used to calculate the composite multipath spread, the composite Doppler spread will be expressed as:

$$v_c = v_{max} - v_{min} \tag{13}$$

[42] An estimation of the SNR is calculated as:

$$SNR = \frac{P|_{A_{sp}} - \rho_n A_{sp}}{\rho_n A_{sp}}, \quad \rho_n = \frac{P|_{\overline{A_{sp}}}}{A_{\overline{sp}}} \tag{14}$$

where A_{sp} represents the area spread factor which is the area of the scattering function over the multipath and Doppler spreads as expressed by *Nissen and Bello* [2003], $P|_{A_{sp}}$ is the power in the area spread factor, $A_{\overline{sp}}$ is the area outside the area of spread factor, $P|_{A_{\overline{sp}}}$ represents the power in the area outside the spread factor area, and ρ_n is the noise power per unit of area in the scattering function.

[43] Figure 10 shows an example of the correlated signal, channel impulse response and scattering function of 18.5 MHz sounding signal at 16:00 UTC. In order to get more practical plot, the axis of the channel impulse response and the scattering function in Figure 10 have been centred.

[44] The high frequency stability of the OCXO unit gives the opportunity to calculate the Doppler frequency shift from the scattering function which is one of the new parameters presented in this paper. The synchronization between the transmitter and the receiver is done by means of the GPS unit. So the propagation time values can be measured from the correlated version of the received signal.

6. Results

[45] As previously stated, this paper is a step forward with respect to the previous soundings presented in *Vilella et al.* [2008]. In that work, a frequency range from 4.6 MHz to 16.6 MHz with an observation period from 18:00 UTC to 11:00 UTC was used. The results presented hereafter are based on measurements over the whole HF Band (2-30 MHz) and throughout 24 hour per day. Moreover, due to significant improvements on the hardware, new measurements of the propagation time and Doppler shift are introduced. All the results are referred to the 2009/2010 survey.

6.1. Narrowband Sounding

[46] As explained in section 4, this analysis focuses on SNR estimation and channel availability, by means of new computing method based on windowing and time framing. Figure 11 is an example of the daily estimation of the SNR for every frequency and hour.

[47] As stated in Section 4, the channel availability means the probability of a link to reach a minimum SNR value and consequently achieve a certain quality of service. Figure 12 represents the channel availability for every frequency and hour. In a first stage, we have considered the ionospheric channel available if 50% of the time frames show SNR higher than 6 dB. As it can be seen, there are some discontinuities that cannot be attributed to the channel behavior.

[48] To overcome this problem, and after further analysis of data, we suggest a new definition of channel availability, considering that the channel is available if 50% of the time frames show a SNR higher than 6 dB and 70% of the time frames show a SNR higher than 3 dB. The channel availability results with the time framing method are shown in Figure 13. The red slots mean that no signal could be detected due to the presence of other strong interfering signals. This fact may not

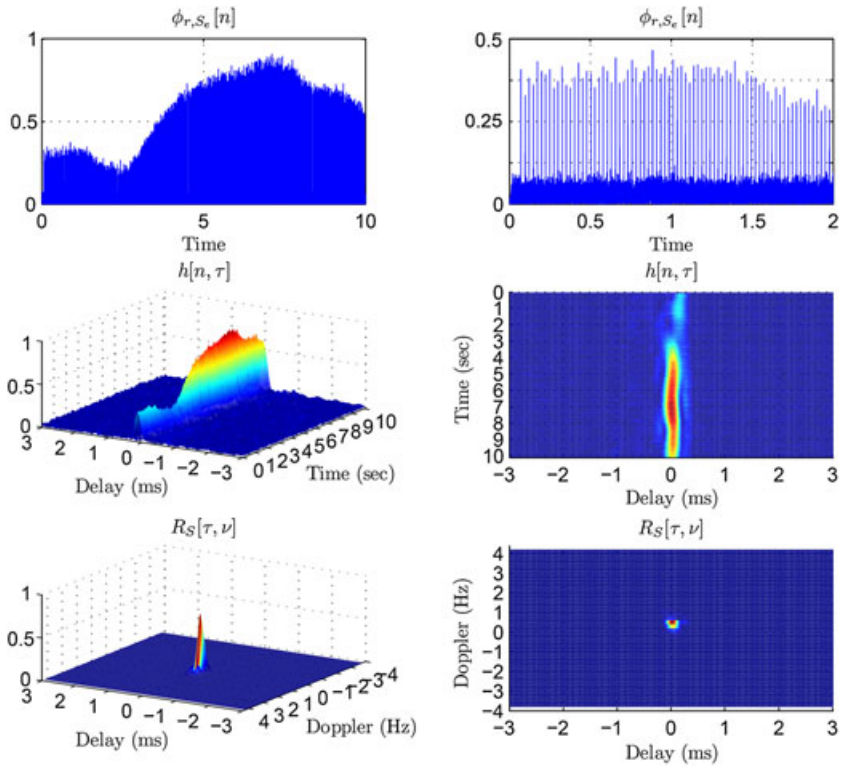

Figure 10. Sounding signal of 18.5 MHz at 16:00 UTC. A correlation of 10 seconds and 2 seconds of the received signal with the original sequence depicted at the top right and left frames respectively. At the middle right and left frame, channel impulse response in 3D and top-view. Scattering function in 3D and top-view are depicted at the bottom right and left frames respectively.

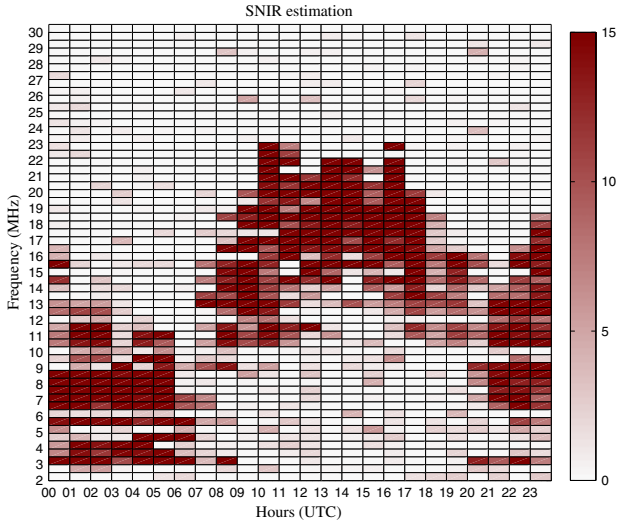

Figure 11. Narrowband SNR estimation as a function of the hour and the frequency of sounding.

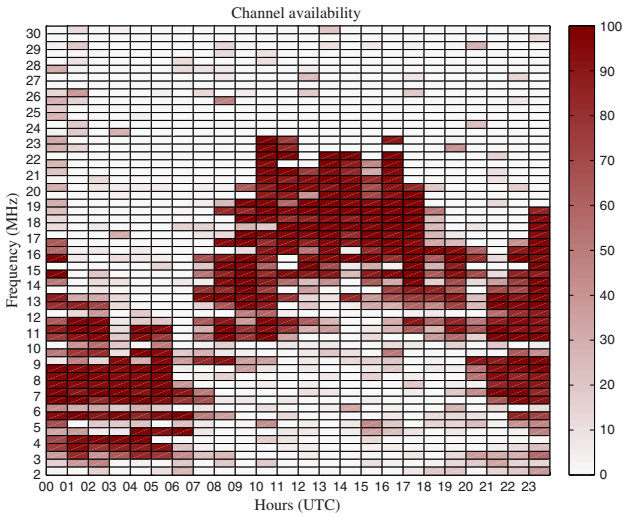

Figure 12. Channel availability which exceeds 6 dB as a function of the hour and the frequency of sounding.

be interpreted as a failure of the method since such signals could not be detected neither by time framing nor by any other technique. According to its position and well-known propagation theories, these red slots should be considered as points of potential availability of the channel. The blue slots mean that the channel is available, i.e., SNR $\geq$ 6 dB the 50% of the time and SNR $\geq$ 3 dB the 70% of the time. The position of the blue slots plus the red slots (global availability) is much more consistent than the availability estimated in previous works carried out by *Vilella et al*. [2008].

[49] Finally we have a small amount of non-detected available slots (green ones), where the method failed to detect the presence of weak signals, and a single false alarm slot (black slot), where the method erroneously detected a good reception.

[50] From Figures 11, 12, and 13, we can distinguish two propagation regions with the following characteristics:

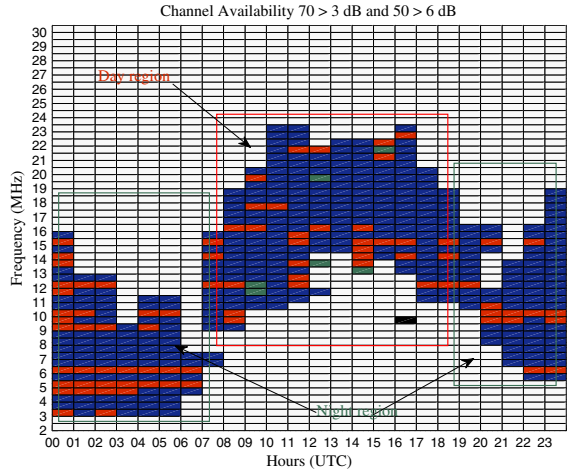

Figure 13. Channel availability with time framing method as a function of the hour and the sounding frequency.

1. The night region. It starts at sunset (around 17:00 UTC) and ends at sunrise (around 07:00 UTC). As sunset extends for four hours and half along the whole path, good propagation conditions exist from 10.5 MHz to 16.5 MHz from 18:00 UTC to 20:00 UTC and it changes to the range from 6.5 MHz to 17.5 MHz from 21:00 UTC to 23:00 UTC. Due to the complete D-layer absence during the night, good propagation conditions exist from 3 MHz to 13 MHz from 0:00 UTC to 7:00 UTC, because all the ionic recombination have been done and the ionosphere is at a steady state. As the sunrise tends to be sudden, likewise is the change to the day region at 7:00 UTC.
2. The day region. It lasts from sunrise (7:00 UTC) to sunset (around 17:00 UTC). The absorption of the D-layer makes propagation of frequencies below 10 MHz impossible. High SNR values can be measured from 10 MHz to 17 MHz from 7:00 UTC to 11:00 UTC, and it changes from 13 MHz to 23.5 MHz from 11:00 UTC to 18:00 UTC. Such a daytime propagation is largely supported by the highly ionization conditions and hence the F2 layer existence.

[51] A clear result is that high frequencies up to 23.5 MHz can be propagated during high solar radiation hours, whereas no data at higher frequencies were gathered during the whole survey.

6.2. Wideband Sounding

[52] As explained in Section 5, this analysis focuses on estimation of scattering function, SNR, composite multipath spread, composite Doppler spread, propagation time, and Doppler frequency shift.

6.2.1. SNR Calculation

[53] An estimation of the wideband SNR derived from the scattering function as computed in Equation 14, is depicted in Figure 14. As expected, there are no significant differences between the wideband and the narrowband SNR estimation of Figure 11.

6.2.2. Composite Multipath Spread

[54] The composite multipath spread is calculated following Equation 11 and the results are shown in Figure 15. Each

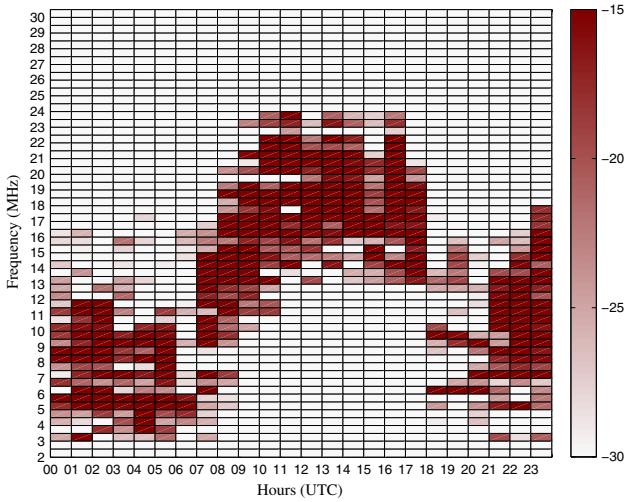

Figure 14. Wideband SNR estimation as a function of the hour and the frequency of sounding.

subfigure represents the multipath spread values obtained over 4 consecutive hours as a function of the sounding frequency. Looking at a summary of data in Table 3, we can state that multipath spread takes values from 3.1 ms to 0.2 ms, decreasing with increasing frequency. The maximum multipath spread values, ranging from 2.7 ms to 3.2 ms have been obtained:

1. In the frequency range from 6 MHz to 14 MHz from 20:00 UTC to 23:00 UTC.
2. In the frequency range from 3 MHz to 14.5 MHz from 00:00 UTC to 03:00 UTC.
3. In the frequency range from 8.5 MHz to 12 MHz at 8:00 UTC, just after sunrise.

[55] The minimum multipath spread of 0.25 ms occurred during the day from 12:00 UTC to 17:00 UTC, in a higher frequency range from 12.5 MHz to 23 MHz. The measurements from 18:00 UTC to 11:00 UTC and 4.5 MHz to 16.5 MHz agree with the results presented by *Vilella et al*. [2008].

6.2.3. Composite Doppler Spread

[56] The composite Doppler spread is calculated as explained in Section 5 and the results are shown in Figure 16. Maximum Doppler spread values from 2 Hz to 2.4 Hz have been measured in the frequency range from 3.5 MHz to 14 MHz from 00:00 UTC to 04:00 UTC.

[57] The Doppler spread values decreased from 2.1 Hz to 0.6 Hz with increasing frequency form 8.5 MHz to 23 MHz, during the time period from 08:00 UTC to 11:00 UTC. As shown in Table 4, minimum Doppler spread values from 0.1 Hz to 0.24 Hz have been measured during the day from 10:00 UTC to 17:00 UTC, in a higher frequency range from 15 MHz to 22.5 MHz.

[58] It is possible to have a better overview of the behavior of the channel looking at the scattering function, that combines information from both multipath spread and Doppler spread in a single graph. The scattering function for several sounding frequencies and hours is shown in Figure 17. As it has been previously mentioned, the ionospheric channel is wide spread both in time and frequency during the night at lower frequencies, while becomes narrow spread in both time and frequency during the day at higher frequencies.

6.3. Propagation Time

[59] The propagation time is the time it takes for the radio wave to travel from SAS to OE (12700 km). An initial approach, assuming a propagation speed equal to $3 * 10^8$ m/s (free space), is:

$$T = 12700 * 10^3 / 3 * 10^8 = 42.3\ ms \tag{15}$$

[60] In practice, we should expect slightly lower propagation speeds, leading to higher propagation times. If we use VOACAP predictions as a first approach, we get propagation times ranging from 42,8 ms to 45,8 ms. In order to measure the propagation time, we have adapted the method mentioned by *Davies* [1990] for measuring the time delay of the first pulse of the received signal. As we are not transmitting RF pulses but PN modulated signals, the time delay of the first correlation peak has been measured. An accurate time reference is needed both in the transmitter and the receiver side, so a new GPS unit with a PPS signal with an accuracy of 1 μs is used.

[61] The average, maximum and minimum values of the propagation time as a function of frequency is shown in Figure 18. As expected, higher average values from 45 ms to 50 ms are obtained. The variation from minimum to maximum values at each frequency is due to the different reflection heights, propagation modes, e.g., four or five hops. In all cases, the real transmission time is slightly higher than the VOACAP prediction.

6.4. Doppler Frequency Shift

[62] Doppler frequency shift arises due to the mobility in the source or destination or any other objects in between that may change the length of the ray as mentioned by *Clarke and Tibble* [1978]. This can be formulated by a shift in the carrier frequency as follows:

$$f_D(t) = \frac{v_a(t)}{\lambda} \tag{16}$$

where $v_a(t)$ is the relative speed of the movement and λ is the wavelength. In our case both the transmitter and the receiver are static, while the reflective ionospheric layers are in continuous movement during the day.

[63] In order to have enough accuracy in our measurement system, an OCXO with a frequency precision of $\pm 30.10^{-9}$ was installed during the 2009/2010 survey. The average Doppler frequency shift as a function of time of day is shown in Figure 19. As expected, the Doppler shift changes are directly related to the changes of ionization of the layers due to the solar radiation. Generally, larger ionization results in reflections at lower heights and shorter ray paths. During the day, Doppler shifts values increase from -4 Hz at 07:00 UTC to 1.2 Hz at 20:00 UTC. During the night, the values are ranging from -0.5 Hz to 1.2 Hz from 20:00 UTC to 06:00 UTC.

[64] We would like to highlight the sudden Doppler shift variations at sunrise. As seen in Figure 19, Doppler shift

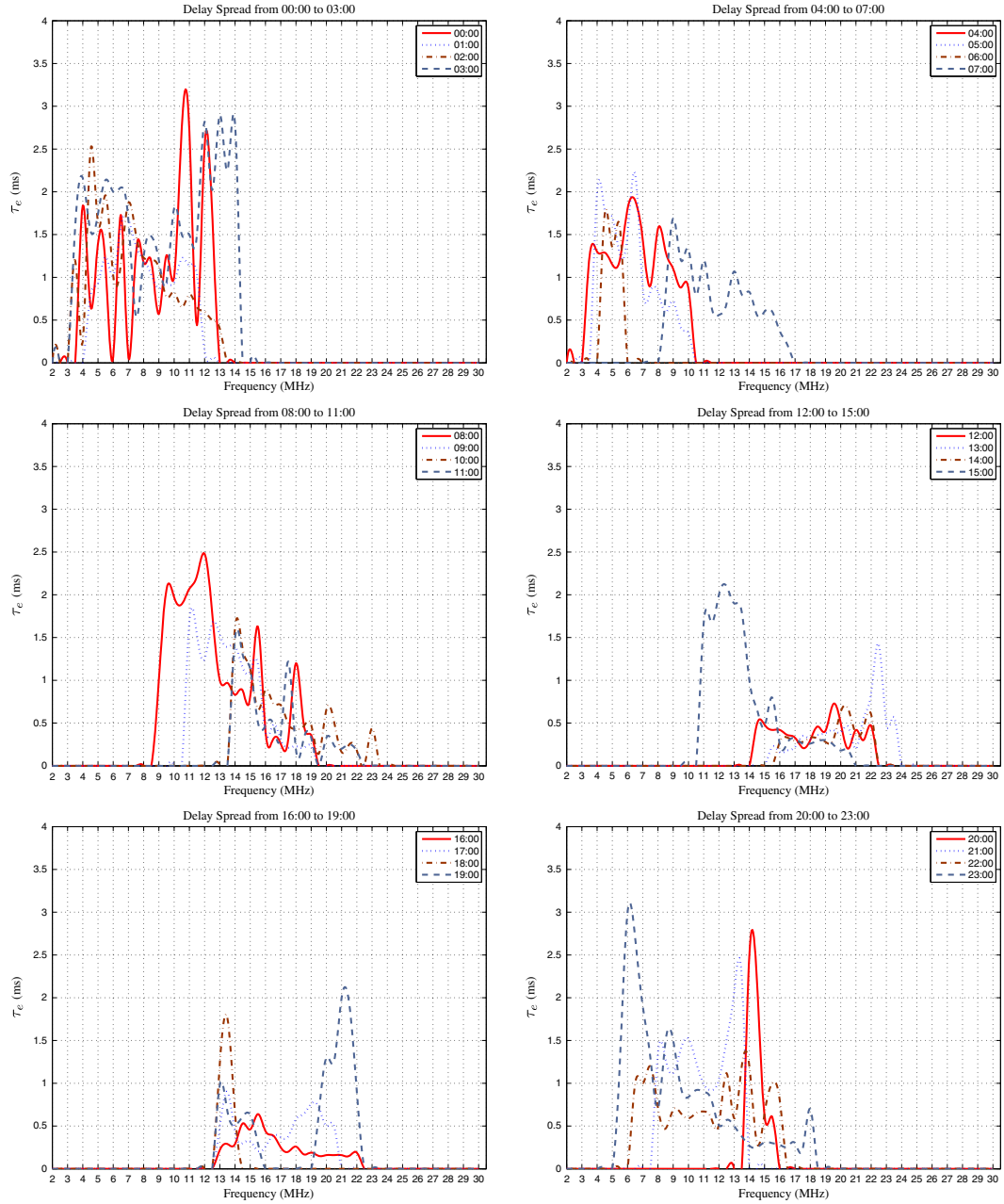

Figure 15. The multipath spread measurements as a function of the sounding frequency and hour.

Table 3. Degradation of the Multipath Spread Values

Hour (UTC)	Start F_c (MHz)	End F_c (MHz)	Max τ_{eff} (ms)	Min τ_{eff} (ms)
05:00	3.5	10.5	2.1	0.4
07:00	8	17	1.6	0.3
08:00	8.5	19.5	2.5	0.2
09:00	10.5	19.5	1.9	0.2
10:00	13.5	23.5	1.7	0.4
11:00	13.5	22.5	1.5	0.25
15:00	10.5	21	2.1	0.2
23:00	5	18.5	3.1	0.6

values suddenly change from -0.5 Hz at 06:00 UTC to -4 Hz at 07:00 UTC, due to the fact that sunrise takes only 24 minutes along the 4 reflection hops as mentioned by *Vilella et al.* [2008]. On the contrary, the sunset takes 4 hours and 24 minutes along the 4 hops. That is the reason for the smooth changes from 17:00 UTC to 21:00 UTC.

7. Concluding Remarks

[65] In this paper, a comprehensive analysis of the channel sounding data gathered from the 2009/2010 campaign between the Spanish Antarctic Station and Ebro Observatory has been presented. Both narrowband and wideband channel parameters have been estimated in the whole HF band, and 24 hours per day, and some new parameters such as the propagation time and the Doppler frequency shift have been included in the set of measurements.

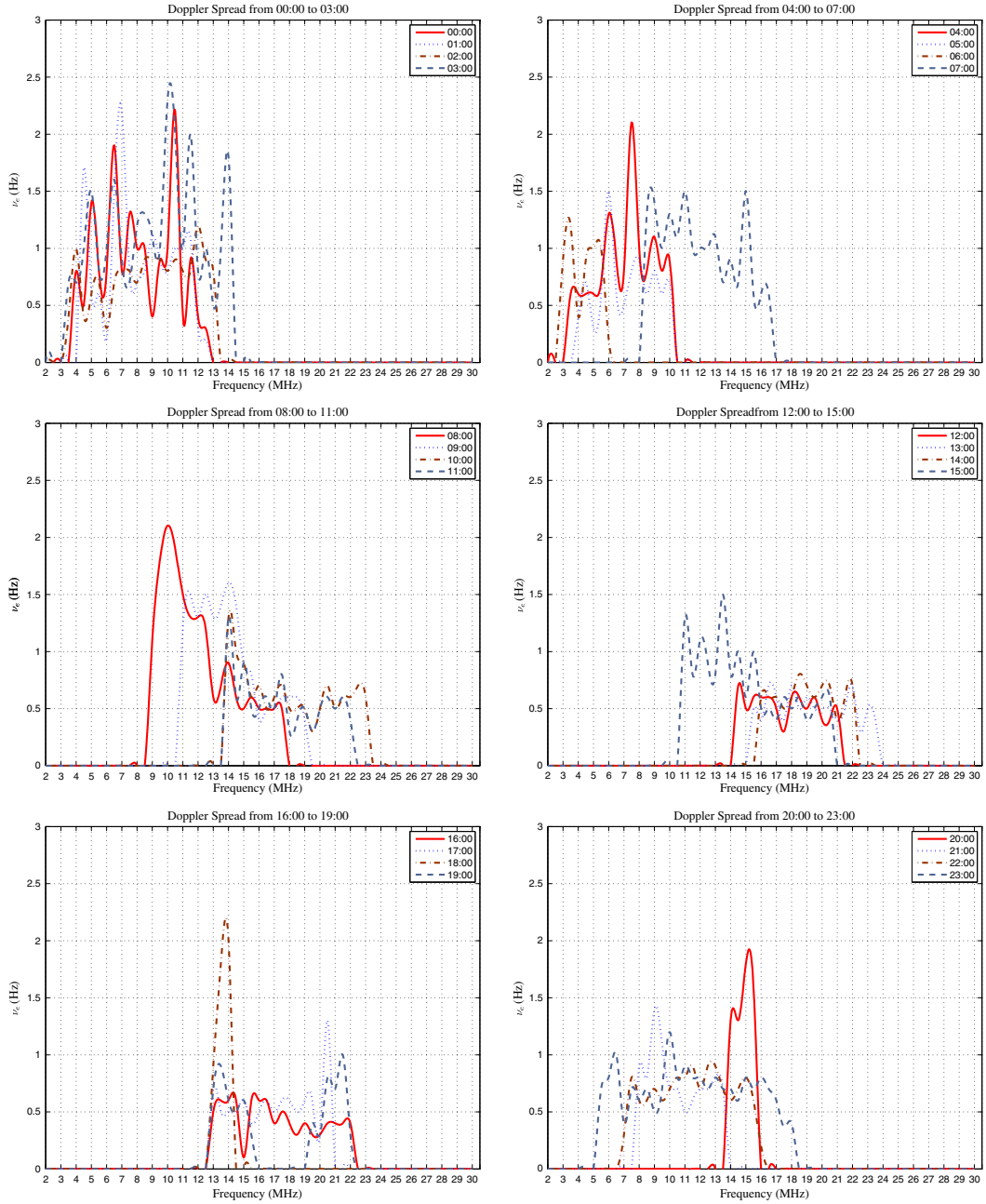

Figure 16. The Doppler spread measurements as a function of the sounding frequency and hour.

Table 4. Minimum Doppler Spread Values

Hour (UTC)	F_c (MHz)	Min v_{eff} (Hz)
10:00	19.5	0.3
11:00	18	0.2
12:00	17.5	0.3
13:00	22.5	0.28
14:00	21	0.4
15:00	19	0.4
16:00	15	0.1
17:00	20	0.2

1. Narrowband Sounding

[66] The windowing filtering techniques have proven to be a key issue in refining the received narrowband signals, being the Kaiser window the best option. We have also introduced a new method to estimate the channel availability, based on the time framing technique in order to mitigate the effect of interfering signals. Concerning the channel availability, two main time and frequency regions have been observed. First, a relevant region of availability exists from 7:00 UTC to the sunset in a frequency range from 10 MHz

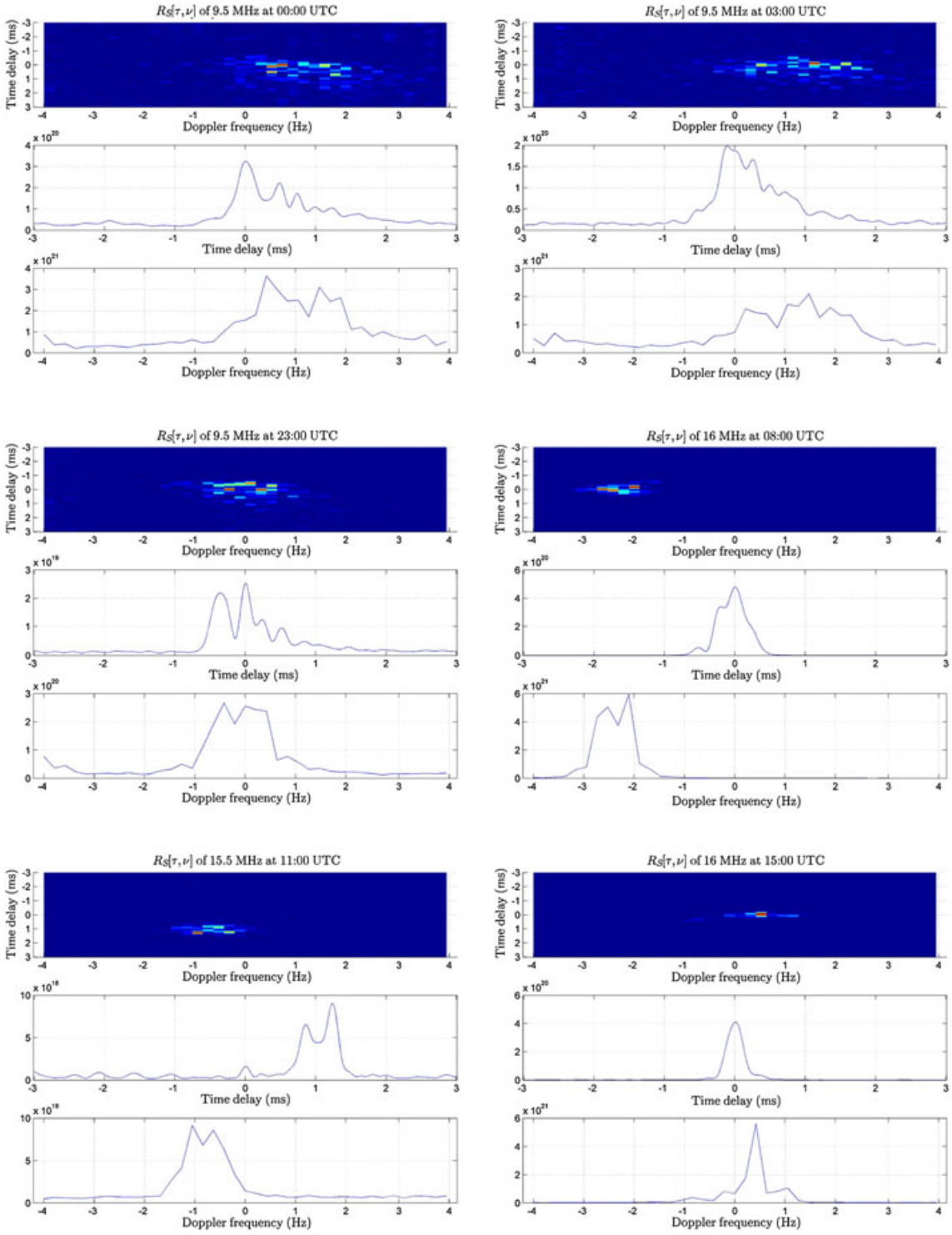

Figure 17. Scattering function and its corresponding delay time and Doppler frequency for different sounding frequencies and times.

to 23 MHz which had not been analyzed before. Second, during the night from 20:00 UTC to 06:00 UTC, the frequencies from 3.5 MHz to 16 MHz show the best degree of availability, in accordance with the results of *Vilella et al*. [2008].

2. Wideband Sounding

[67] The multipath spread values show clear differences between night and day. The maximum multipath spread values have been obtained from 20:00 UTC to 3:00 UTC and just after sunrise at frequencies lower than 14 MHz, while the minimum values were observed during the day from 12:00 UTC to 17:00 UTC, in a higher frequency range from 12.5 MHz to 23 MHz.

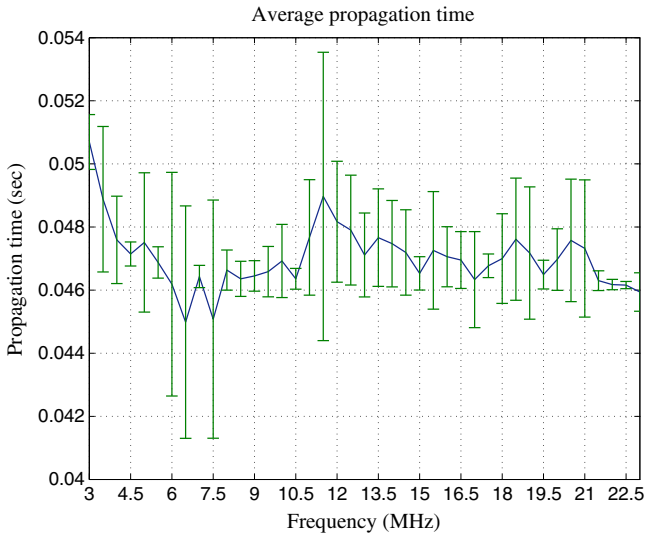

Figure 18. Average propagation time as a function of sounding frequencies.

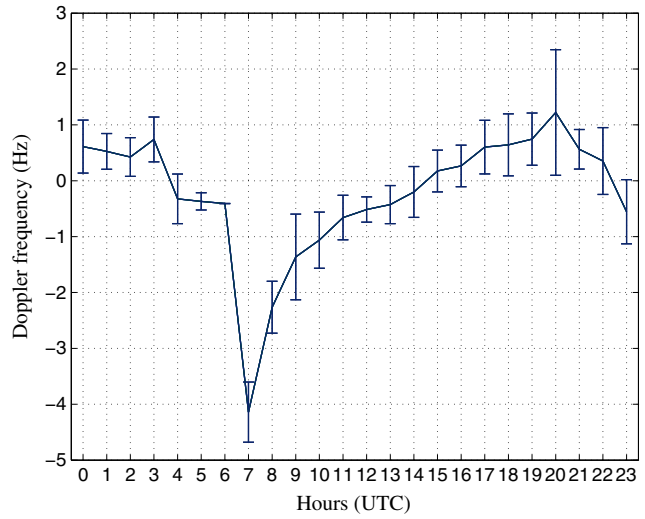

Figure 19. Average Doppler frequency shift during the 24 hours.

3. Propagation Time

[68] Average propagation time values ranging from 45 ms to 50 ms have been measured which is slightly higher than the theoretical one. The variation of the propagation time depend on the propagation path of the wave.

4. Doppler Frequency Shift

[69] The motion of the ionospheric layers causes a Doppler frequency shift, that varies from -4 Hz to 1.2 Hz during the day and from -0.5 Hz to 1.2 Hz during the night. It is remarkable the sudden change at 07:00 UTC due to the sunrise.

[70] **Acknowledgments.** This work has been funded by the Spanish Government under the projects CGL2006-12437-C02-01, CTM2008-03536-E, CTM2009-13843-C02-02 and CTM2010-21312-C03-03. A. G. Ads has an FPI grant of BES-2008-00948 from the Spanish Government. The authors would like to thank D. Altadill for his important guidance.

References

Angling, M. J., and N. C. Davies (1997), On an ionospheric channel simulator driven by measurements of multipath and Doppler spread, in *Proc. IEE Colloquium on, Propagation Characteristics and Related System Techniques for Beyond Line-of Sight Radio, 1997*(390), pp. 4(1–6), doi:10.1049/ic:19971351.

Angling, M., P. Cannon, N. Davies, T. Willink, V. Jodalen, and B. Lundborg (1998), Measurements of Doppler and Multipath spread on oblique high latitude HF paths and their use in characterizing data modem performance, *Radio Sci.*, *33*(1), pp. 97–107, doi:10.1029/97RS02206.

Bergadà, P., M. Deumal, C. Vilella, J. R. Regué, D. Altadill, and S. Marsal (2009), Remote Sensing and Skywave Digital Communication from Antarctica, *Sensors*, *9*, pp. 10136–10157, 2009, doi:10.3390/s91210136.

Blackman, R. B., J. Tukey, and J. Wilder (1959), Particular Pairs of Windows, *The Measurement of Power Spectra, From the Point of View of Communications Engineering*, pp. 98–99, Dover Publications, New York, USA.

Clarke, R. H., and D. V. Tibble (1978), Measurement of the elevation angles of arrival of multicomponent H.F. skywaves, in *Proc. Institution of Electrical Engineers*, *125*(1), pp. 17–24, January, 1978, doi:10.1109/ICCSN.2009.55.

Davies, K. (1990), *Ionoshperic Radio*, Peter Peregrines Ltd., London, UK.

Fitzgerald, J., P. Argo, and R. Carlos (1999), Equatorial spread F effects on an HF path: Doppler spread, spatial coherence, and frequency coherence, *Radio Sci.*, *34*(1), pp. 167–178, doi:10.1029/1998RS900013.

Goodman, J., J. Ballard, and E. Sharp (1997), A long-term investigation of the HF communication channel over middle- and high-latitudes paths, *Radio Sci.*, *32*(4), pp. 1705–1715, doi:10.1029/97RS01194.

Houpis, H., and L. Nickisch (1991), An ionospheric propagation prediction method for low latitudes and mid-latitudes, *Radio Sci.*, *26*(4), pp. 1049–1057, doi:10.1029/91RS00491.

Kaiser, J. F. (1974), Nonrecursive Digital Filter Design Using the I_0 − sinh window function, in *Proc. IEEE International Sump. on, Circuits and Systems*, pp. 20–23, April, 1974.

Mastrangelo, J. F., J. J. Lemmon, L. E. Vogler, J. A. Hoffmeyer, L. E. Pratt, and C. J. Behm (1997), A New Wideband High Frequency Channel Simulation System, *IEEE Transactions on Communications*, *45*(1), pp. 26–34, doi:10.1109/26.554283.

Nissen, C. A., and P. A. Bello (2003), Measured channel parameters for the disturbed wide-bandwidth HF channel, *Radio Sci.*, *38*(2), pp. 1023, doi:10.1029/2002RS002746.

Oppenheim, A. V., and R. W. Shafer (1989), *Discrete-time Signal Processing*, Prentice Hall, pp. 444–447, Upper Saddle River, New Jersey, USA.

Parsons, J. D. (2000), *Mobile Radio Propagation channel*, John Wiley and Sons, New York, USA.

Proakis, J. (2001), *Digital Communications*, pp. 807, McGraw-Hill New York.

Vilella, C., D. Miralles, J. Socoró, L. Pijoan, and R. Aquilué (2005), A new sounding system for HF digital communications from Antarctica, in *Proc. International symposium on, Antennas and Propagation*, pp. 419–422, August, 2005, Seoul, South Korea.

Vilella, C., P. Bergadà, M. Deumal, L. Pijoan, and R. Aquilué (2006), Transceiver architecture and Digital Down Converter design for long distance, low power HF ionospheric links, in *Proc. Ionospheric Radio Systems and Techniques*, pp. 95–99, London, 18- 21 July, doi:10.1049/cp:20060311.

Vilella, C., D. Miralles, and L. Pijoan (2008), An Antarctica-to-Spain HF ionospheric radio link: sounding results, *Radio Sci.*, *43*, RS4008, doi:10.1029/2007RS003812.

Vogler, L. E., and J. A. Hoffmeyer (1993), A model for wideband HF propagation channels, *Radio Sci.*, *28*(6), pp. 1131–1142, doi:10.1029/93RS01607.

Warrington, E. M. (1998), Observations of the directional characteristics of ionospherically propagated HF radio channel sounding signals over two high latitude paths, *IEE Proceedings, Microwaves, Antennas and Propagation 145*(5), pp. 379–385, October, 1998, doi:10.1049/ip-map:19982068.

Warrington, E. M., and A. J. Stocker (2003), Measurements of the Doppler and Multipath spread of the HF signals received over a path oriented along the midlatitude trough, *Radio Sci.*, *38*(5), pp. 1080, doi:10.1029/2002RS002815.

Watterson, C. C., J. Juroshek, and W. D. Bensema (1970), Experimental configuration of an HF channel model, *IEEE Transactions on Communication Technology*, *18*(6), pp. 792–803, December, 1970, doi:10.1109/TCOM.1970.1090438.